Structural Engineering and Mechanics, *Vol. 68, No. 4 (2018) 385-398*
DOI: https://doi.org/10.12989/sem.2018.68.4.385

The use of the strain approach to develop a new consistent triangular thin flat shell finite element with drilling rotation

Hamza Guenfoud*[1], Mohamed Himeur[1a], Hassina Ziou[2a] and Mohamed Guenfoud[1b]

[1]LGCH Laboratory, 8 Mai 1945 University of Guelma, Algeria
[2]Mohamed Khider University, Biskra, Algeria

(Received December 19, 2017, Revised September 24, 2018, Accepted September 26, 2018)

Abstract. In the present paper, we offer a new flat shell finite element. It is the result of the combination of a membrane element and a bending element, both based on the strain-based formulation. It is known that C° plane membrane elements provide poor deflection and stress for problems where bending is dominant. In addition, they encounter continuity and compliance problems when they connect to C1 class plate elements. The reach of the present work is to surmount these problems when a membrane element is coupled with a thin plate element in order to construct a shell element. The membrane element used is a triangular element with four nodes, three nodes at the vertices of the triangle and the fourth one at its barycenter. Each node has three degrees of freedom, two translations and one rotation around the normal. The coefficients related to the degrees of freedom at the internal node are subsequently removed from the element stiffness matrix by using the static condensation technique. The interpolation functions of strain, displacements and stresses fields are developed from equilibrium conditions. The plate element used for the construction of the present shell element is a triangular four-node thin plate element based on Kirchhoff plate theory, the strain approach, the four fictitious node, the static condensation and the analytic integration. The shell element result of this combination is robust, competitive and efficient.

Keywords: finite element method; membrane; plate; shell; condensation; deformation approach; drilling rotation

1. Introduction

Complex shell structures are regularly encountered in diverse fields. The development of simple and efficient finite elements for the analysis of these structures is a main push of scientific research in solid mechanics. Flat shell finite elements are derived by the superposition of plate elements with plane stress elements, in which the membrane and plate bending properties are decoupled (for isotropic materials). In the literature, it is revealed that shell elements provide good accuracy for both displacement and stress of thin and thick structures. Nevertheless, problems are often encountered, making it difficult to achieve the assigned objectives. However, if membrane elements are combined with a plate bending element, they affect the accuracy of the results because of the poor performance of the membrane elements for dominated bending problems, which require a fine mesh density, and they induce continuity and compliance problems during the transition to shell elements.

The main observed constraints are often linked to the following:

– Displacement fields incompatibility aspects when affixing the membrane elements to those of the plate.

– The two phenomena of “shear locking” and “membrane locking”.

– The numerical problems induced by the absence of the “sixth DOF” in the case of co-planar elements.

– The numerical problems associated with numerical integration.

Many finite elements have been developed for solving these problems. However, most of them have remained ineffective in the analysis of arbitrary geometric configurations. Isoparametric elements are the most successful among those available, due to their ability to successfully model curved structures. From the literature review, some researchers are addressing these problems. Bhothikhun and Dechaumphai (2014) have developed the Discrete Kirchhoff Triangle (DKT) plate-bending element together with the CST membrane. An adaptive meshing technique is applied to improve the solution accuracy and to decrease the computational effort. The formulations of a triangular element (THS) and a quadrilateral element (QHS) based on a hybrid variational principle and Rezaiee-Pajand and Karkon (2014) have obtained analytical homogeneous solution of the thin plate equation. Jeon *et al.* (2014) present an improvement of a scheme to enrich the three-node triangular MITC shell finite element by interpolation cover functions. The enhancement scheme increases the solution accuracy without any traditional local mesh refinement. Rezaiee-Pajand and Yaghoobi (2014) developed a new triangular element, named SST10. The formulation uses the optimization constraints of insensitivity to distortion and rotational invariance. In addition, the equilibrium equations

*Corresponding author, Ph.D. Student
E-mail: Guenfoud.hamza@univ-guelma.dz or hamzaguenfoud@gmail.com
[a]Ph.D.
[b]Professor

ISSN: 1225-4568 (Print), 1598-6217 (Online)

are established based on some constraints among the strain states. Kugler *et al.* (2010), Boutagouga (2008, 2016) and Hamadi (2016) have developed a new quadrilateral membrane finite element with drilling degrees of freedom. It is based on a variational principle employing an independent rotation field in the order of the normal of a plane continuum element. Further studies on the triangular finite element have also been published: Sabir (1985), Barik and Mukhopadhyay (2002), Kim and Bathe (2009), Papanicolopulos *et al.* (2009), Burkardt (2010), Serpik (2010), Huang *et al.* (2010), Gileva *et al.* (2013) and Himeur (2008, 2015). In 1990 Batoz and Dhatt developed triangular membrane finite elements with three nodes and six nodes called T3 (CST) and T6, correspondingly. Belarbi (2000) has also developed many triangular finite elements, namely the SBT2, SBT2v, SBT3 and SBT3v. Chinosi (2005) has made several amendments to the boundary conditions for Mindlin-Reissner plates. In recent times, Shin and Lee (2014) developed a three-node triangular flat shell element based on the assumed natural deviatory strain formulation for enhanced use in curved shell geometries. The strain approach technique is applied to the derivation of the membrane stiffness of the proposed element. The scope of the present research is to surmount the problem that appears when combining plane membrane elements of class C^0 with plate elements of class C^1.

Therefore, the aim of the present work is the formulation of a thin flat shell finite element based on the “deformation approach” in order to avoid these difficulties on the one hand, and the construction of a thin flat finite shell element, which is simple and competent for the analysis of complex structures, on the other hand. To accomplish this, we have enriched our approach with the concepts and development techniques based on:

– The adoption of the “deformation approach”,

– The introduction of a “fictitious fourth node”,

– The elimination of the freedom degrees corresponding to the “fictitious fourth node” by static condensation,

– The use of “analytic integration” to evaluate the stiffness matrix.

Earlier, Himeur and Guenfoud (2008, 2015) led to the construction of a triangular membrane finite element, which can be easily shared with inflected elements (slabs, beams and shells). “T43_Eq” by Himeur and Guenfoud (2008, 2015) is a membrane triangular finite element with a central disrupted node. It is characterized by the presence of an unidentified nodal rotation defined by the derivation of displacement fields (drilling rotation). The interpolation functions are those obtained from the equilibrium conditions (bi-harmonic polynomials chosen from the solutions given by Teodorescu (1982) based on Airy function development). These interpolation functions are developed by using Pascal’s triangle. The “T43_Eq” element has three nodes positioned at the summit with three degrees of freedom, and a fourth fictitious node situated in the center of the triangle is added.

We use the bending triangular finite element, founded on the Kirchhoff’s thin plate theory, with a fictitious fourth node based on the strain approach developed by Himeur and Guenfoud (2011) to construct the present shell element. This element is planned by using the strain approach. The interpolation functions of the deformation fields (consequently, displacements and stresses) are developed by using Pascal’s triangle. The considered element is a triangular element to which we added a fourth fictitious node positioned external to and away from the triangle. This position, outside, is thus chosen to avoid the relaxation of the stiffness matrix resulting in an excessive estimation of the nodal displacements.

For both, the membrane and the plate element formulation, we eliminate, the degrees of freedom corresponding to the fourth fictitious node, using the static condensation method applied on the basic stiffness matrix at the elementary level. Hence, the main significance of the fictitious node lies in the improvement of the displacement field (P refinement i.e., increasing the degree of the polynomial interpolation), which accordingly leads to a better precision of the approximate solution. The corresponding variationally criterion used in the present formulation is the virtual work principle. The analytical integration to evaluate the elementary stiffness matrix is extremely interesting in order to avoid the defeat of convergence phenomenon observed when using the numerical integration (in this case the convergence trained by regular and undistorted meshes) for the formulation of the isoparametric elements.

2. The membrane element (four node triangular element)

The membrane element, designated T43_Eq, is formulated using the strain approach of Himeur and Guenfoud (2008). The interpolation functions of strain fields, and thus displacements and stresses, are developed from the equilibrium conditions. Fig. 1 presents this element. Every node has three degrees of freedom: two translations U and V and the rotation about the normal (“drilling rotation”) θ_z. Consequently, the displacement fields have twelve independent constants ($a_1,\ldots,a_{12}$). The relationship between strains and displacements is given as follows

$$\varepsilon_x = \frac{\partial U}{\partial x} \qquad \varepsilon_y = \frac{\partial V}{\partial y} \qquad \gamma_{xy} = \frac{\partial U}{\partial y} + \frac{\partial V}{\partial x} \tag{2.1}$$

The true rotation around the normal, (the “drilling rotation”) θ_z, is given by the relation

$$\theta_z = \frac{1}{2}.\left(\frac{\partial V}{\partial x} - \frac{\partial U}{\partial y}\right) \tag{2.2}$$

The following system gives the equilibrium conditions

$$\begin{bmatrix} \frac{\partial}{\partial x} & 0 & \frac{\partial}{\partial y} \\ 0 & \frac{\partial}{\partial y} & \frac{\partial}{\partial x} \end{bmatrix} . \begin{Bmatrix} \sigma_x \\ \sigma_y \\ \tau_{xy} \end{Bmatrix} + \begin{Bmatrix} f_x \\ f_y \end{Bmatrix} = \begin{Bmatrix} 0 \\ 0 \end{Bmatrix} \tag{2.3}$$

The Hooke’s law for isotropic materials Eqs. (2.4) offers

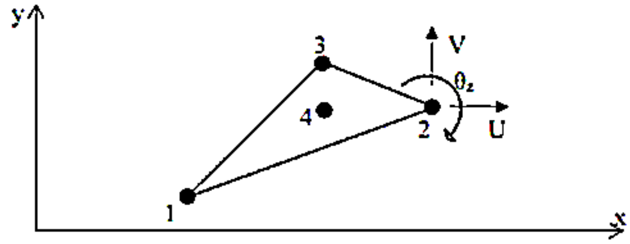

Fig. 1 Triangular four-node element "T43_Eq"

the relationship between stresses and strains at the plane stresses state

$$\begin{Bmatrix}\sigma_x\\ \sigma_y\\ \tau_{xy}\end{Bmatrix}=\frac{E}{1-\nu^2}\begin{bmatrix}1 & \nu & 0\\ \nu & 1 & 0\\ 0 & 0 & \frac{1-\nu}{2}\end{bmatrix}\begin{Bmatrix}\varepsilon_x\\ \varepsilon_y\\ \gamma_{xy}\end{Bmatrix}\text{ Else}$$

$$\begin{Bmatrix}\varepsilon_x\\ \varepsilon_y\\ \gamma_{xy}\end{Bmatrix}=\frac{1}{E}\begin{bmatrix}1 & -\nu & 0\\ -\nu & 1 & 0\\ 0 & 0 & \frac{E}{G}\end{bmatrix}\begin{Bmatrix}\sigma_x\\ \sigma_y\\ \tau_{xy}\end{Bmatrix} \tag{2.4}$$

For zero volume forces, the approximation functions are selected by introducing the Airy function F(x,y), which condenses the problem of relation (2.3) to a bi-harmonic equation (Himeur and Guenfoud 2015)

$$\nabla^4 F(x,y)=0 \tag{2.5}$$

Using

$$\sigma_x=\frac{\partial^2 F(x,y)}{\partial y^2}\quad \sigma_y=\frac{\partial^2 F(x,y)}{\partial x^2}\quad \tau_x=\frac{\partial^2 F(x,y)}{\partial x\partial y} \tag{2.6}$$

If we substitute Eq. (2.6) into Equation systems (2.4), the strains become as follows

$$\varepsilon_x=\frac{1}{E}\left(\frac{\partial^2 F(x,y)}{\partial y^2}-\nu.\frac{\partial^2 F(x,y)}{\partial x^2}\right)$$

$$\varepsilon_y=\frac{1}{E}\left(-\nu\frac{\partial^2 F(x,y)}{\partial y^2}+\frac{\partial^2 F(x,y)}{\partial x^2}\right) \tag{2.7}$$

$$\gamma_{xy}=-\frac{1}{G}.\left(\frac{\partial^2 F(x,y)}{\partial x\partial y}\right)$$

Consequently, the universal solution of Eq. (2.5) standing on the bi-harmonic polynomials is the opening point for getting the stress, strain and displacement. Zweiling (1952) determines these bi-harmonic polynomials. To formulate the strain field approximation, the first twelve bi-harmonic polynomials are assumed. These fields are as follows:

- For Rigid Body Motions (RBM), the strains are zero. So, ε

$$\varepsilon_x=0\qquad \varepsilon_y=0\qquad \gamma_{xy}=0 \tag{2.8}$$

For the higher modes, we are

$$\begin{cases}E.\varepsilon_x=a_4-2.a_7.\nu.y+2a_8.x-6.a_9\nu.x+6.a_{10}y-6a_{11}.\nu.x.y+6.a_{12}.x.y\\ E.\varepsilon_y=a_5+2.a_7.y-2.a_8.\nu\nu.+6a_9.x-6.a_{10}.\nu\nu.+6a_{11}.x.y-6a_{12}.\nu.x.y\\ E.\gamma_{xy}=2.a_6-4.a_7(1+\nu)x-4.a_8(1+\nu)y-6.a_{11}(1+\nu)x^2-6.a_{12}(1+\nu)y^2\end{cases} \tag{2.9}$$

This resultant field is characterized by:

- The existence of constant strains that guarantee the convergence and the homogeneous strain when the mesh is refined, represented by constants a_4, a_5, and a_6.
- The existence of linear strains at dilations (ε_x , ε_y) and a state of linear strains of distortions (γ_{xy}), corresponding to the parameters a_7, a_8, which put distortions in dependence with dilations.
- The higher strains of distortions, symbolized by the parameters a_{11}, a_{12}.
- The agreement of the general equation of strains compatibility.

$$\frac{\partial^2\varepsilon_x}{\partial y^2}+\frac{\partial^2\varepsilon_y}{\partial x^2}-\frac{\partial^2\gamma_{xy}}{\partial x\partial y}=0 \tag{2.10}$$

The approval of the universal equation of strains compatibility is verified through the Airy function, as follows

$$\begin{aligned}&\frac{\partial^2\varepsilon_x}{\partial y^2}=\frac{\partial^2}{\partial y^2}\left(\frac{1}{E}\left(\frac{\partial^2 F(x,y)}{\partial y^2}-\nu\frac{\partial^2 F(x,y)}{\partial x^2}\right)\right)\Rightarrow\frac{1}{E}\left(\frac{\partial^4 F(x,y)}{\partial y^4}-\nu\frac{\partial^4 F(x,y)}{\partial x^2\partial y^2}\right)\\ &\frac{\partial^2\varepsilon_y}{\partial x^2}=\frac{\partial^2}{\partial x^2}\left(\frac{1}{E}\left(\frac{\partial^2 F(x,y)}{\partial x^2}-\nu\frac{\partial^2 F(x,y)}{\partial y^2}\right)\right)\Rightarrow\frac{1}{E}\left(\frac{\partial^4 F(x,y)}{\partial x^4}-\nu\frac{\partial^4 F(x,y)}{\partial x^2\partial y^2}\right)\\ &-\frac{\partial^2\gamma xy}{\partial x\partial y}=-\frac{\partial^2}{\partial x\partial y}\left(\frac{2(1+\nu)}{E}\left(-\frac{\partial^2 F(x,y)}{\partial x\partial y}\right)\right)\Rightarrow\frac{2(1+\nu)}{E}\left(\frac{\partial^4 F(x,y)}{\partial x^2\partial y^2}\right)\\ &=\frac{1}{E}\left(\frac{\partial^4 F(x,y)}{\partial y^4}+\frac{\partial^4 F(x,y)}{\partial x^4}+2\frac{\partial^4 F(x,y)}{\partial x^2\partial y^2}\right)=\frac{1}{E}\nabla F^4(x,y)=0\end{aligned} \tag{2.11}$$

Finally, the integration of strain fields provides the following displacement fields

$$\begin{cases}E.u=a_1-a_3.y+a_4.x+a_6.y-2.a_7.\nu.x.y+a_8.(x^2-y^2(2+\nu))-3.a_9(\nu.x^2+y^2)\\ \quad+6.a_{10}x.y-a_{11}.(3.\nu.x^2.y+y^3)+a_{12}.(3.x^2.y-y^3(2+\nu))\\ E.v=a_2+a_3.x+a_5.y+a_6.x+a_7.(y^2-x^2(2+\nu))-2.a_8.\nu.x.y+6a_9.x.y\\ \quad-3.a_{10}.(\nu.y^2+x^2)+a_{11}.(3.x.y^2-x^3.(2+\nu))-a_{12}.(3.\nu.x.y^2+x^3)\\ E.\theta.=a_3-2.a_7.x+2.a_8.y+6.a_9.y-6.a_{10}.x+3.a_{11}(y^2-x^2)+3a_{12}(y^2-x^2)\end{cases} \tag{2.12}$$

In matrix form, the resultant displacement field represented by Eq. (2.12) can be written as

$$\begin{Bmatrix}u(x.y)\\ v(x,y)\\ \theta_Z(x,y)\end{Bmatrix}=\frac{1}{E}[f(x.y)]\{a_i\} \tag{2.13}$$

With

$$\{a_i\}^T=\langle a_1,a_2,a_3,a_4,a_5,a_6,a_7,a_8,a_9,a_{10},a_{11},a_{12}\rangle$$

$$[f(x,y)]=\begin{bmatrix}1 & 0 & -y & x & 0 & y & -2\nu xy & (x^2-y^2(2+\nu)) & -3(\nu x^2+y^2) & 6xy & (-3\nu x^2y-y^3) & (3x^2y-y^3(2+\nu))\\ 0 & 1 & x & 0 & y & x & (y^2-x^2(2+\nu)) & -2\nu xy & 6xy & -3(\nu y^2+x^2) & (3y^2x-x^3(2+\nu)) & (-3\nu y^2x-x^3)\\ 0 & 0 & 1 & 0 & 0 & 0 & -2x & 2y & 6y & -6x & 3(y^2-x^2) & 3(y^2-x^2)\end{bmatrix} \tag{2.14}$$

Having recognized the four nodal coordinates (x_j, y_j) corresponding to node j (i = 1,...,4) and affecting the relation (2.13), the displacements nodal vector at the elementary level is obtained by

$$\left\{q^e\right\}=\frac{1}{E}\begin{bmatrix}[f(x_1.y_1)]\\ [f(x_2.y_2)]\\ [f(x_3.y_3)]\\ [f(x_4.y_4)]\end{bmatrix}\left\{a_i\right\} \tag{2.15}$$

With

$$\left\{q^e\right\}^T =< u_1, v_1, \theta z_1, u_2, v_2, \theta z_2, u_3, v_3, \theta z_3, u_4, v_4, \theta z_4 >$$

and $\frac{1}{E}\begin{bmatrix}[f(x_1.y_1)]\\ [f(x_2.y_2)]\\ [f(x_3.y_3)]\\ [f(x_4.y_4)]\end{bmatrix}$ Is the element nodal coordinates matrix designated by [*A*].

Himeur and Guenfoud (2008, 2008, 2015) detail the improvement of the matrix [A] for the finite element "T43_Eq". Finally, we obtain the interpolation functions of displacements from Eq. (2.15) by the evaluation of the parameters 'a_i'

$$\left\{a_i\right\}=[A]^{-1}\left\{q^e\right\} \tag{2.16}$$

Substituting Eq. (2.16) into Eq. (2.14), we get the relation between the vector displacement and the nodal displacement by the following relationship

$$\begin{Bmatrix}u(x.y)\\ v(x,y)\\ \theta_Z(x,y)\end{Bmatrix}=\frac{1}{E}\left[f(x.y)\right].[A]^{-1}\left\{q^e\right\} \tag{2.17}$$

$\frac{1}{E}\left[f(x.y)\right].[A]^{-1}=[N]$ represents the matrix shape function N_i.

In the case of plane stress, the linear strain tensor representing the strain-displacement relationship is given by

$$\begin{Bmatrix}\varepsilon_x\\ \varepsilon_y\\ \gamma_{xy}\end{Bmatrix}=\begin{bmatrix}\frac{\partial}{\partial x} & 0\\ 0 & \frac{\partial}{\partial y}\\ \frac{\partial}{\partial y} & \frac{\partial}{\partial x}\end{bmatrix}.\begin{Bmatrix}u(x,y)\\ v(x,y)\end{Bmatrix} \tag{2.18}$$

Replacing u and v by their values of Eq. (2.17), the strain-displacement relation (2.18) takes the following form

$$E.\begin{Bmatrix}\varepsilon_x\\ \varepsilon_y\\ \gamma_{xy}\end{Bmatrix}=\begin{bmatrix}0&0&0&1&0&0&-2\nu\nu&2x&-6\nu\nu&6y&-6\nu\nu x&6xy\\ 0&0&0&0&1&0&2y&-2\nu\nu&6x&-6\nu\nu&6xy&-6\nu\nu x\\ 0&0&0&0&0&2&-4x(1+\nu)&-4y(1+\nu)&0&0&-6x^2(1+\nu)&-6y^2(1+\nu)\end{bmatrix}.\left\{a_i\right\} \tag{2.19}$$

Therefore, the strain matrix will take the form

$$[Q]=\frac{1}{E}\begin{bmatrix}0&0&0&1&0&0&-2\nu\nu&2x&-6\nu\nu&6y&-6\nu\nu x&6xy\\ 0&0&0&0&1&0&2y&-2\nu\nu&6x&-6\nu\nu&6xy&-6\nu\nu x\\ 0&0&0&0&0&2&-4x(1+\nu)&-4y(1+\nu)&0&0&-6x^2(1+\nu)&-6y^2(1+\nu)\end{bmatrix} \tag{2.20}$$

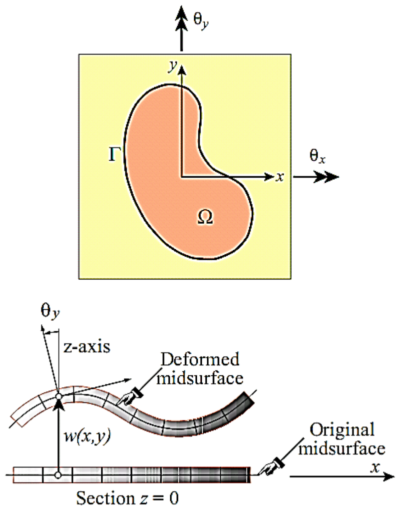

Fig. 2 Deformation of a bending Kirchhoff thin plate

3. The Kirchhoff thin plate element

3.1 Fundamental equations of thin plate theory (Kirchhoff theory)

3.1.1 Kinematics equations compatibility conditions

Fig. 2 presents the rotations around the two axes x and y denoted by θ_x and θ_y respectively and the slopes (gradients) in both directions defined by the variables β_x and β_y; with

$$\beta_x=\theta_y \qquad \beta_y=-\theta_x \tag{3.1}$$

The hypothesis of the plane cross-section involves a linear variation of the displacement above the thickness of the plate, and is interpreted by

$$\begin{aligned}u(x,y,z)&=z\beta_x(x,y)=z\theta_y(x,y)\\ v(x,y,z)&=z\beta_y(x,y)=-z\theta_x(x,y)\\ w(x,y,z)&=w(x,y)\end{aligned} \tag{3.2}$$

The expressions (3.2) make it legitimate to disconnect the membrane displacement (u, v) and the transverse bending displacement (w) in reference to the Kirchhoff hypothesis. The displacement field to describe the behaviour of the plate is described as

$$u=-z\frac{\partial w}{\partial x} \qquad v=-z\frac{\partial w}{\partial y} \tag{3.3}$$

The relations between the rotations and the curvatures are given by

$$-\theta_x=\beta_y=-\frac{\partial w}{\partial y} \qquad \theta_y=\beta_x=-\frac{\partial w}{\partial x} \tag{3.4}$$

By deriving the displacement field, the infinitesimal strain tensor is then obtained as

$$\begin{aligned}\varepsilon_x&=\frac{\partial u}{\partial x}=z\frac{\partial \beta_x}{\partial x}=-z\frac{\partial^2 w}{\partial x^2}\\ \varepsilon_y&=\frac{\partial v}{\partial y}=z\frac{\partial \beta_y}{\partial y}=-z\frac{\partial^2 w}{\partial y^2}\\ \gamma_{xy}&=\frac{\partial u}{\partial y}+\frac{\partial v}{\partial x}=z(\frac{\partial \beta_x}{\partial y}+\frac{\partial \beta_y}{\partial x})=-2z\frac{\partial^2 w}{\partial x\partial y}\end{aligned} \tag{3.5}$$

where $\gamma_{xz} = \gamma_{yz} = 0$ according to the Kirchhoff hypothesis.

The relations between the moments and bending curvatures are expressed by

$$
\begin{aligned}
K_x &= \frac{\partial \beta_x}{\partial x} = -\frac{\partial^2 w}{\partial x^2} \\
K_y &= \frac{\partial \beta_y}{\partial y} = -\frac{\partial^2 w}{\partial y^2} \\
K_{xy} &= (\frac{\partial \beta_x}{\partial y} + \frac{\partial \beta_y}{\partial x}) = -2\frac{\partial^2 w}{\partial x \partial y}
\end{aligned}
\tag{3.6}
$$

Saint-Venant (1854) established the compatibility conditions (Frey 2000). Their agreement is required to assure the uniqueness of the solution. The compatibility equations are developed as follows

$$
\begin{aligned}
&\frac{\partial^2 K_x}{\partial y^2} + \frac{\partial^2 K_y}{\partial x^2} = \frac{\partial^2 K_{xy}}{\partial x \partial y} \\
&\frac{\partial^2 \gamma_{xz}}{\partial x \partial y} - \frac{\partial^2 \gamma_{yz}}{\partial x^2} + \frac{\partial^2 K_{xy}}{\partial x} = 2\frac{\partial K_x}{\partial y} \\
&\frac{\partial^2 \gamma_{yz}}{\partial x \partial y} - \frac{\partial^2 \gamma_{xz}}{\partial y^2} + \frac{\partial^2 K_{xy}}{\partial y} = 2\frac{\partial K_y}{\partial x}
\end{aligned}
\tag{3.7}
$$

3.1.2 Constitutive law

The constitutive law, in the case of plane state stress and for isotropic material, is written as

$$
\begin{Bmatrix} \sigma_x \\ \sigma_y \\ \tau_{xy} \end{Bmatrix} = \frac{E}{1-\nu^2} \begin{bmatrix} 1 & \nu & 0 \\ \nu & 1 & 0 \\ 0 & 0 & \frac{1-\nu}{2} \end{bmatrix} \begin{Bmatrix} \varepsilon_x \\ \varepsilon_y \\ \gamma_{xy} \end{Bmatrix} \tag{3.8}
$$

In terms of the *moment-curvature* relationship, Eq. (3.8) is written as

$$
\begin{Bmatrix} M_x \\ M_y \\ M_{xy} \end{Bmatrix} = \frac{Eh^3}{12(1-v^2)} \begin{bmatrix} 1 & v & 0 \\ v & 1 & 0 \\ 0 & 0 & \frac{1-v}{2} \end{bmatrix} \begin{Bmatrix} K_x \\ K_y \\ K_{xy} \end{Bmatrix} \quad \begin{Bmatrix} M_x \\ M_y \\ M_{xy} \end{Bmatrix} = \frac{Eh^3}{12(1-v^2)} \begin{bmatrix} 1 & v & 0 \\ v & 1 & 0 \\ 0 & 0 & \frac{1-v}{2} \end{bmatrix} \begin{Bmatrix} -\frac{\partial^2 w}{\partial x^2} \\ -\frac{\partial^2 w}{\partial y^2} \\ -2\frac{\partial^2 w}{\partial x \partial y} \end{Bmatrix} \tag{3.9}
$$

3.1.3 Equations of equilibrium

The balance between the internal and external actions of an element with dimensions dx×dy in equilibrium state is obtained by the following equation

$$
q dx dy + (Q_x + \frac{\partial Q_x}{\partial x}) dy + (Q_y + \frac{\partial Q_y}{\partial y}) dx - Q_x dy - Q_y dx = 0 \tag{3.10}
$$

where Q_x and Q_y are the shear actions forces in the sections perpendicular to the x and y axes respectively. The expression (3.10) is simplified to become

$$
q + \frac{\partial Q_x}{\partial x} + \frac{\partial Q_y}{\partial y} = 0 \tag{3.11}
$$

The equilibrium of moments about the *x* and *y* axes delivers

$$
Q_x = \frac{\partial M_x}{\partial x} + \frac{\partial M_{xy}}{\partial y} \qquad Q_y = \frac{\partial M_y}{\partial y} + \frac{\partial M_{xy}}{\partial x} \tag{3.12}
$$

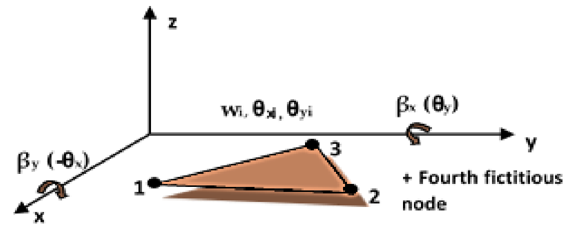

Fig. 3 Triangular Kirchhoff thin plate element with w, β_x, β_y degrees of freedom at each node

By substituting the Q_x and Q_y values of Eqs. (3.12) in Eq. (3.11) and using the bending behaviour law (3.9), the balance condition will result in the displacement function "w" by the following relation

$$
\frac{\partial^4 w}{\partial x^4} + 2\frac{\partial^4 w}{\partial x^2 \partial y^2} + \frac{\partial^4 w}{\partial y^4} - \frac{q}{D} = 0 \tag{3.13}
$$

With $D = \dfrac{Eh^3}{12(1-\upsilon^2)}$

3.2 The "Himeur" Kirchhoff thin plate finite element

3.2.1 Bending shapes functions

The bending curvatures are equal to zero for Rigid Body Motions (RBM)

$$
\kappa_x = 0 \qquad \kappa_y = 0 \qquad \kappa_{xy} = 0 \tag{3.14}
$$

By changing in Eqs. (3.6) the curves with their values given by Eqs. (3.14) and then integrating, we get the displacement fields signifying the rigid body motions, which are as follows

$$
W = a_1 - a_2.x - a_3 y \quad \beta_x = a_2 \quad \beta_y = a_3 \tag{3.15}
$$

with a_2 and a_3, parameters representing rotations θ_x and θ_y of the rigid body around the respective axis "*y*" and "*x*" and a_1, parameter signifying the transverse displacement of the rigid body along the normal (axis "*z*") representing the translation.

The element has four nodes (see Fig. 3): three heads to which we have added a fourth imaginary node. All the nodes have three degrees of freedom. Hence the displacement fields, expressed by the use of the model deformation, have twelve independent constant parameters (a_1, ..., a_{12}). The first three (a_1, a_2, a_3) are used in Eqs. (3.15) to represent rigid body motions (RBM). The other nine (a_4, ..., a_{12}) are used to characterise the state of pure bending. They share in the deformation interpolation functions to satisfy the balance relations (3.7) of kinematic compatibility for plane elasticity. Consequently, the flexure curvature fields for the higher modes derive from Pascal's triangle as follows

$$
\begin{aligned}
\kappa_x &= a_4 + a_5.x + a_6.y + a_7.x.y \\
\kappa_y &= a_8 + a_9.x + a_{10}.y + a_{11}x.y \\
\kappa_{xy} &= a_{12} + 2.a_6.x + a_7.x^2 + 2.a_9.y + a_{11}.y^2
\end{aligned}
\tag{3.16}
$$

By substituting in Eqs. (3.6) the curvatures with their values given by Eqs. (3.16) with subsequent integration, we obtain the complete displacement field for the bending mode

$$\begin{aligned} W &= -a_4.\frac{x^2}{2} - a_5.\frac{x^3}{6} - a_6.\frac{x^2.y}{2} - a_7.\frac{x^3.y}{6} - a_8.\frac{y^2}{2} - a_9.\frac{x.y^2}{2} - a_{10}.\frac{y^3}{6} - a_{11}.\frac{x.y^3}{6} - a_{12}.\frac{x.y}{2} \\ \beta_x &= a_4.x + a_5.\frac{x^2}{2} + a_6.x.y + a_7.\frac{x^2.y}{2} + a_9.\frac{y^2}{2} + a_{11}.\frac{y^3}{6} + a_{12}.\frac{y}{2} \\ \beta_y &= a_6.\frac{x^2}{2} + a_7.\frac{x^3}{6} + a_8.y + a_9.x.y + a_{10}.\frac{y^2}{2} + a_{11}.\frac{x.y^2}{2} + a_{12}.\frac{x}{2} \end{aligned} \tag{3.17}$$

By adding the relations (3.15) and (3.17), we obtain the final field (for rigid body motions and the pure bending deformation) of displacements

$$\begin{aligned} W &= a_1 - a_2.x - a_3.y - a_4.\frac{x^2}{2} - a_5.\frac{x^3}{6} - a_6.\frac{x^2.y}{2} - a_7.\frac{x^3.y}{6} - a_8.\frac{y^2}{2} - a_9.\frac{x.y^2}{2} - a_{10}.\frac{y^3}{6} - a_{11}.\frac{x.y^3}{6} - a_{12}.\frac{x.y}{2} \\ \beta_x &= a_2 + a_4.x + a_5.\frac{x^2}{2} + a_6.x.y + a_7.\frac{x^2.y}{2} + a_9.\frac{y^2}{2} + a_{11}.\frac{y^3}{6} + a_{12}.\frac{y}{2} \\ \beta_y &= a_3 + a_6.\frac{x^2}{2} + a_7.\frac{x^3}{6} + a_8.y + a_9.x.y + a_{10}.\frac{y^2}{2} + a_{11}.\frac{x.y^2}{2} + a_{12}.\frac{x}{2} \end{aligned} \tag{3.18}$$

We write the displacement field given by Eqs. (3.18) in the matrix form as follows

$$\begin{Bmatrix} W(x, y) \\ \beta_x(x, y) \\ \beta_y(x, y) \end{Bmatrix} = \left[f(x, y)\right]\{a_i\} \tag{3.19}$$

With, $\{a_i\}^T = < a_1, a_2, a_3, a_4, a_5, a_6, a_7, a_8, a_9, a_{10}, a_{11}, a_{12} >$

$$[f(x, y)] = \begin{bmatrix} 1 & -x & -y & -\frac{x^2}{2} & -\frac{x^3}{6} & -\frac{x^2.y}{2} & -\frac{x^3.y}{6} & -\frac{y^2}{2} & -\frac{x.y^2}{2} & -\frac{y^3}{6} & -\frac{x.y^3}{6} & -\frac{x.y}{2} \\ 0 & 1 & 0 & x & \frac{x^2}{2} & x.y & \frac{x^2.y}{2} & 0 & \frac{y^2}{2} & 0 & \frac{y^3}{6} & \frac{y}{2} \\ 0 & 0 & 1 & 0 & 0 & \frac{x^2}{2} & \frac{x^3}{6} & y & x.y & \frac{y^2}{2} & \frac{x.y^2}{2} & \frac{x}{2} \end{bmatrix} \tag{3.20}$$

The nodal displacements vector, at the elementary level, corresponding to the nodes j (j = 1... 4), is obtained by applying the relation (3.20) after recognising the nodal coordinates (x_j, y_j)

$$\{q^e\} = \begin{bmatrix} [f(x_1, y_1)] \\ [f(x_2, y_2)] \\ [f(x_3, y_3)] \\ [f(x_4, y_4)] \end{bmatrix} \{a_i\} \tag{3.21}$$

With,

$\{q^e\}^T = < w_1, \beta_{x1}, \beta_{y1}, w_2, \beta_{x2}, \beta_{y2}, w_3, \beta_{x3}, \beta_{y3}, w_4, \beta_{x4}, \beta_{y4} >$

$[A] = \begin{bmatrix} [f(x_1, y_1)] \\ [f(x_2, y_2)] \\ [f(x_3, y_3)] \\ [f(x_4, y_4)] \end{bmatrix}$ is the nodal coordinate's matrix (Appendix A1 in Himeur *et al*. 2011).

From relation (3.21), we gather the value of parameters "a_i" by the following system

$$\{a_i\} = [A]^{-1}\{q^e\} \tag{3.22}$$

By replacing the parameters, which have the relationship given by (3.22), in the equation system (3.19), we obtain the following relationship

$$\begin{Bmatrix} W(x, y) \\ \beta_x(x, y) \\ \beta_y(x, y) \end{Bmatrix} = \left[f(x, y)\right].[A]^{-1}.\{q^e\} \tag{3.23}$$

which represents the interpolation functions matrix N_i.

The strain-displacement relationship takes the following expanded form by replacing in Eqs. (3.6) the *w(x,y)* values of Eq. (3.19)

$$\{K\} = \begin{Bmatrix} K_x \\ K_y \\ K_{xy} \end{Bmatrix} = \begin{bmatrix} 0 & 0 & 0 & 1 & x & y & x.y & 0 & 0 & 0 & 0 & 0 \\ 0 & 0 & 0 & 0 & 0 & 0 & 0 & 1 & x & y & x.y & 0 \\ 0 & 0 & 0 & 0 & 0 & 2.x & x^2 & 0 & 2.y & 0 & y^2 & 1 \end{bmatrix} . \{a_i\} \tag{3.24}$$

Finally, the deformation matrix [Q(x,y)] is assumed as follows ([K]=[Q(x,y)]{a_i})

$$[Q(x, y)] = \begin{bmatrix} 0 & 0 & 0 & 1 & x & y & x.y & 0 & 0 & 0 & 0 & 0 \\ 0 & 0 & 0 & 0 & 0 & 0 & 0 & 1 & x & y & x.y & 0 \\ 0 & 0 & 0 & 0 & 0 & 2.x & x^2 & 0 & 2.y & 0 & y^2 & 1 \end{bmatrix} \tag{3.25}$$

4. Elementary stiffness matrix for both membrane and plate element

The elementary discredited internal virtual work is given by the expression

$$\left(\delta W_{int}\right)^e = \int_{V^e} \delta\{\varepsilon\}^T.[\sigma].dV \tag{4.1}$$

Knowing that

$$\{\varepsilon\} = \left[N'\right]\{q^e\} = \left[Q(x, y)\right].[A]^{-1}\{q^e\} \tag{4.2}$$

And

$$\{\sigma\} = [D].\{\varepsilon\} \tag{4.3}$$

Moreover, substituting in Expression (4.1) $\{\varepsilon\}$ and $\{\sigma\}$ by values given respectively in Eqs. (4.2) and (4.3) produce

$$\left(\delta W_{int}\right)^e = \delta\{q^e\}^T \int_V \left[Q(x, y)\right]^T.[A^{-1}]^T.[D].\left[Q(x, y)\right].[A]^{-1}\{q^e\}dV \tag{4.4}$$

Consequently, the following integrating form obtains the elementary stiffness matrix derived from Expression (4.4), for both membrane and bending elements

$$[K^e] = \int_V \left[Q(x, y)\right]^T.[A^{-1}]^T.[D].\left[Q(x, y)\right].[A]^{-1}dV \tag{4.5}$$

The expression (4.5) can be written as

$$[K^e] = [A^{-1}]^T \int_V \left[Q(x, y)\right]^T [D].\left[Q(x, y)\right].dV.[A]^{-1} = [A^{-1}]^T [K_o].[A]^{-1} \tag{4.6}$$

The evaluation of the $[K_0]$ expression is determined by analytic integration in Belarbi (1999), Hamadi (2006), and Himeur (2008) of the different components of the resulting matrix product $\left[Q(x, y)\right]^T[D].\left[Q(x, y)\right]$, whose expressions take the form "$H_{\alpha\beta} = C.x^{\alpha}.y^{\beta}$". In conclusion, the elementary stiffness matrix, to be considered at the assembly and construction of the global stiffness matrix of the membrane and plate structure, is acquired after condensation of the matrix [K^e]. The static condensation relates at the degrees of freedom to the fictitious fourth

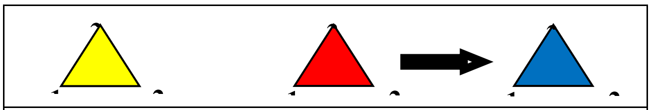

Membrane element	Kirchhoff Thin Plate Bending element	Shell element
9 DOF	**9 DOF**	**18 DOF**
$\{u_1\ v_1\ \theta z_1\ u_2\ v_2\ \theta z_2\ u_3\ v_3\ \theta z_3\}^T$	$\{w_1\ \theta_{x1}\ \theta_{y1}\ w_2\ \theta_{x2}\ \theta_{y2}\ u_3\ \theta_{x3}\ \theta_{y3}\}^T$	**18 DOF**
T43_Eq	*HIMEUR*	***Shell element***

Fig. 4 Construction mode of the shell element

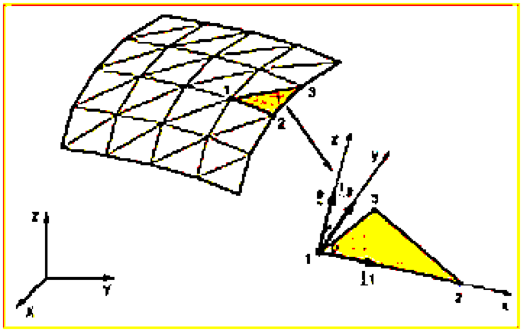

Fig. 5 The shell element relative to the local (its own) and global coordinates

node (Himeur and Guenfoud 2008, 2008, 2011, 2014, 2015).

5. The result flat plane thin shell element

The present element is a flat plane thin shell element, obtained by superimposing the T43_Eq. membrane finite element (Himeur 2008) with the Himeur thin plate finite element (Himeur 2011). For the isotropic material case, we obtain the elementary stiffness matrix by adding the stiffness matrix of the membrane element to that of the bending element without a coupling effect. We outline the approach with this principle as follows:

* We approximate the real geometry with flat planes (Fig. 5), so we neglect the curvatures on the element. This avoids the membrane locking.

* Use of a membrane element coupled to that of a plate-bending element (Fig. 4).

* The shell element may have any orientation in the global coordinate system XYZ (Fig. 5).

* We establish the passage of the local coordinates to the global coordinates through the rotation matrix [R_o] as follows

$$[K_e]\{u\}=[R_O]^T[K_e][R_O]\{U\} \tag{5.1}$$

* We rearrange the local rigidity terms (18×18) before assembly in the local level as in Fig. 6.

With:

Membrane rigidity term

Bending rigidity term

We remove the difficulty associated with the rigidity in θz in the formulation of the membrane element by introducing the rotation around the normal "drilling rotation" in the construction of the corresponding elementary stiffness matrix.

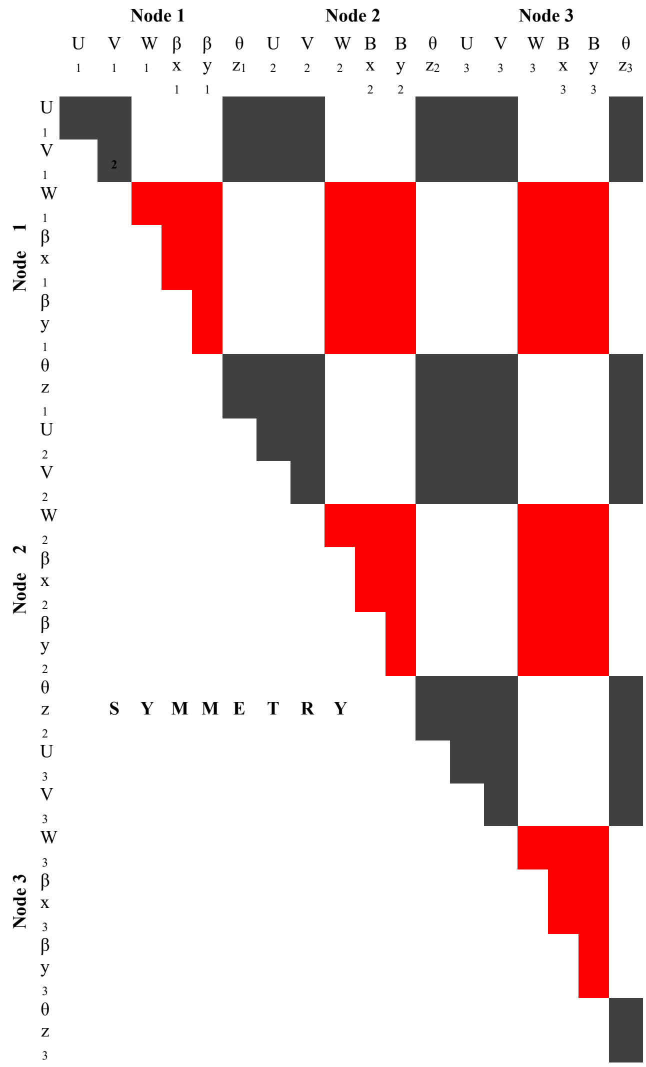

Fig. 6 Structural type of the elementary shell rigidity in the local coordinates [Ke]

6. Validation tests

We examine a number of commonly used benchmark problems to compare the present element with other elements models in the open literature to assess their relative accuracy and convergence. We summarize as follows the elements to be included in the comparisons:

Name Element Description

ANST3: Three-node shell element based on assumed covariant strains (Guenfoud 1990).

ANST6: Six-node shell element based on assumed covariant strains (Guenfoud 1990).

ECB1: A three-node deep shell theory (Geoffroy 1983).

ECB2: A three-node shallow shell theory (Geoffroy 1983).

DKTM: A three-node thin shallow shell element based on Marguerre's theory (El-Khaldi 1987).

DSTCOQ: Three-node flat shell element (Guenfoud 1996, 2000).

DSTM: Three-node thick shallow shell element based on Marguerre's theory (Guenfoud 1996, 2000).

DKT12: (CST+DKT6) (Batoz 1990).

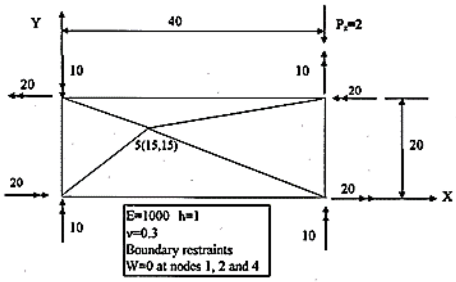

Fig. 7 Standard Kirchhoff Patch-Test

DKT18: (CST+DKT9) (Batoz 1990).
DLR18: (Carpenter 1986).
ACM_RSBES: (Hamadi 2016).
ACM_SBQ4: (Belarbi 2000).

6.1 Spectral analysis of stiffness matrix

The evaluation of the eigenvalues of the stiffness matrix of the present element was performed for various element shapes. Upon performing a spectral analysis of the present element stiffness matrix, we reveal six zero eigenvalues associated with the requisite rigid body modes. No spurious zero energy modes are present, as one would expect from an analytical and exactly integrated stiffness matrix. Therefore, the stiffness matrix has a correct rank and the element is considered as kinematically consistent.

6.2 Patch test

6.2.1 The standard Kirchhoff patch test

We assume the standard Kirchhoff plate patch test described as follows in Fig. 7. A thin, rectangular plate is subjected to a bending state such that all three-moment resultants are constant throughout the plate domain. The plate discretization consisting of four geometrically distinct elements produced exact values of all three constant moments in respect of the element.

6.2.2 Inextensional bending modes

In order to investigate membrane locking, we perform a rectangular plate with initial out-of-flatness subjected to constant bending. In the first case, the initial out-of-flatness is $W_0 = \frac{4Hx}{L}\left(1 - \frac{x}{L}\right)$ and in the second case it is $W_0 = \frac{Hxy}{BL}$. We analyze the test with H=0.1 and 1. The analytical solution, according to Marguerre's theory, is given in Guenfoud (1993). In all cases, the error is less than 1.1% for the energy. The maximum membrane stress is equal to 2.9% of the flexural stress for H=1, and is less than 1.1% of the flexural stress for H=0.1. We comprehend that the element does not lock. If we did not pay special attention to membrane locking, the results would be very modest.

6.3 Pinched cylinder with free edges problem

The pinched cylinder is a classical problem that is used extensively to check the ability of shell elements to represent the inextensional bending deformation. This is the example that is most common in the literature. Indeed, since 1967 it has always served researchers (Thomas 1975, Zienkiewicz 1977, Batoz 1977, Geoffroy 1983, Carpenter 1986, Guenfoud 1990, 1996) to evaluate the performance of the finished shell elements for a convergence rate perspective and representation of rigid body motion. The test relates to the analysis of an isotropic pinched cylinder with short free edges as shown in Fig. 8. The open-ended cylinder leads to pure inextensional deformation at the limit as h/R approaches zero. For the present example, we have h/R=0.0031 and h/L=0.0015, indicating that the cylinder is very thin. Fig. 8 shows the model geometry and mechanical data structure. The upload relates to the mid-section of the cylinder by the application of two diametrically opposite forces (P) and (-P).

Length of the cylinder (*L*)	10.35
Radius of the cylinder (*R*)	4.953
Young's Modulus (*E*)	10.50×10^6
Poisson Coefficient (υ)	0.3125
Thickness (h)	0.01548
Load (concentrated P)	0.10

Due to dual symmetry, we model only one-eighth ABCD of the cylinder by imposing the symmetry conditions along the edges "AB", "CB" and "DC". The limits conditions considered here are as follows

$W = \theta_x = \theta_y = 0$	Along AB
$V = \theta_x = \theta_z = 0$	Along CB
$U = \theta_y = \theta_z = 0$	Along DC

The considered mesh is composed of a single mesh (double triangular element) in the longitudinal direction, since the shell deforms substantially in the same manner in each cross-section, and several meshes are considered in the circumferential direction. The results L/h=668.6 and R/h=320 indicate that the shell is very thin. Timoshenko and Woinowsky-Krieger (1959) give an analytical solution for this limiting case (thin deep shell), which is W_C = -0.0244. We compare our results with those given by Guenfoud (1990, 1996).

We note that for the present test the bending mode (flexion) is dominant. Indeed, at point B, for example, we have for z = h/2 that : $\sigma_x(z) = \frac{N_x}{h} + M_x.\frac{12}{h^3}.z$ $\quad \sigma_x(z = \frac{h}{2}) = \frac{N_x}{h} + M_x.\frac{12}{h^3}.\frac{h}{2}$

From where: $\frac{M_x}{N_x} = \frac{5}{6}h$

The criterion considered for evaluating the performance of the present shell element for the actual example is the displacement along the z-axis of the point C (displacement W_C) and the radial displacement at point B (displacement U_B). We present in Figs. 9 and 10 the results of our element and we conclude:

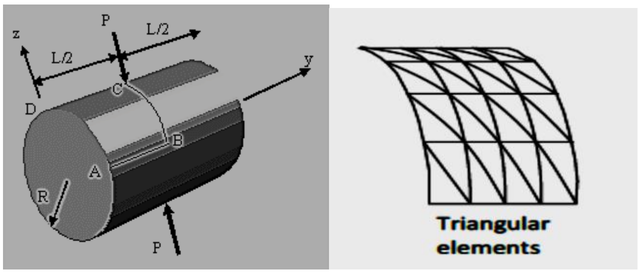

Fig. 8 Pinched cylinder with free edges

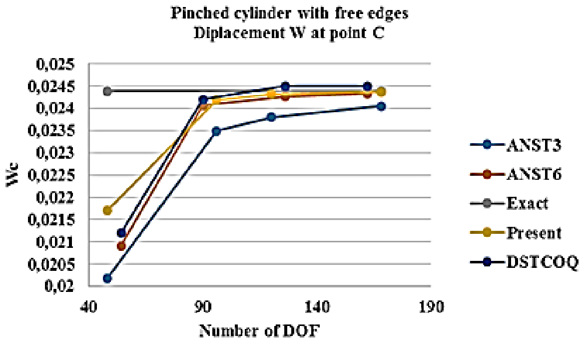

Fig. 9 Pinched Cylinder with free edges-Displacement W at Node C

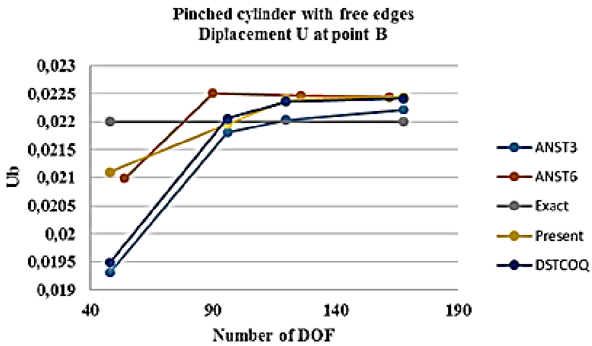

Fig. 10 Pinched Cylinder with free edges-Displacement U at Node B

- There is a rapid convergence of the present element, reflecting a correct representation of the state of rigid body motions.
- Our element converges to the solution given by the deep shell theory W_C = -0.0244 (thin cylinder case).
- With the selected mesh, we observe a monotonic upward convergence of the present element.
- Numerical results for the pinched cylinder with open ends indicate that the proposed element exhibits a good accuracy.

6.4 Infinitely long pinched cylinder

The infinitely long pinched circular cylinder, presented in Fig. 11, is subjected to two opposite uniform transverse load lines. We seek to solve this problem so as to demonstrate the influence of the relationships between deformations and displacements on the one hand, and to follow our element behaviour while modelling curved structures on the other hand.

Radius of the cylinder (R)	10
Young's Modulus (E)	10^5
Poisson Coefficient (υ)	0
Thickness (h)	1

$V = \theta_x = 0$	On all nodes
$U = \theta_y = 0$	Along EF and DC

We present the geometrical and mechanical data of this shell in Fig. 11. As in Batoz (1977) and Geoffroy (1983) and based on symmetry, we model only a quarter EAFDBC of a shell strip considering several cuts (Fig. 11). The conditions of the imposed limits allow us to eliminate the influence of the Y direction on the deformation of the whole. Punctual forces substitute the uniform load. We present the normalized numerical results of upright displacements for the A and B nodes according to the total number of degrees of freedom in Figs. 12 and 13. We compare the present element results to two exact solutions. The first, given by Donnel (1933), is based on the shallow shell theory and the second one is based on the deep shell theory given by Koiter (1960, 1973) and Sander (1959), as well as on the numerical results presented by Guenfoud (1990) and Geoffroy (1983).

It is worth noting that:

- A rapid monotonous convergence towards the exact solution is obtained by our element.
- We notice the existence of a jump between the first two mesh sizes and the third. This is due to the fact that the shell behaves as a shallow one for the two first meshes, while it shows a deep shell behaviour if the mesh is refined.

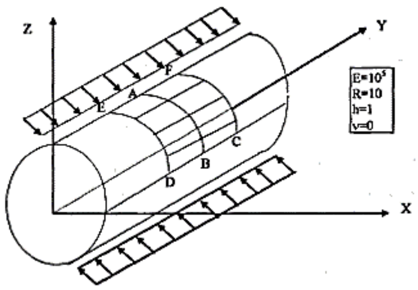

Fig. 11 Infinitely long pinched cylinder

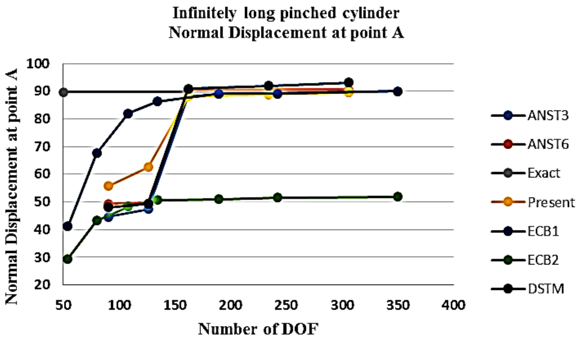

Fig. 12 Infinitely long pinched cylinder-normal displacement at node A

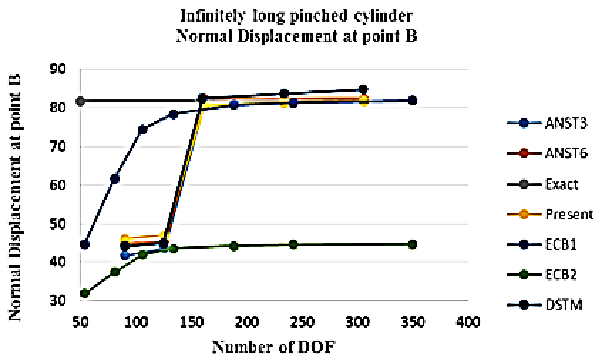

Fig. 13 Infinitely long pinched cylinder-normal displacement at node B

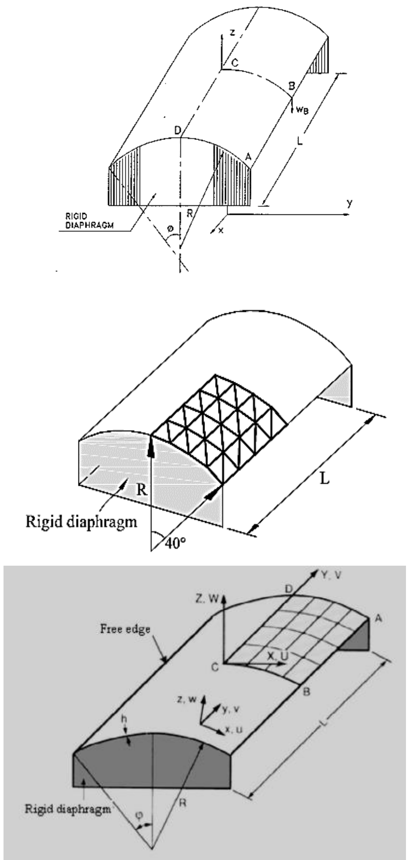

Fig. 14 Cylindrical panel subjected to its weight-Scordelis-Lo roof, thin shallow shell

6.5 Cylindrical panel subjected to its weight (Scordelis-Lo roof, thin shallow shell)

The next test considered here and frequently used to investigate the performance of a shell element is the Scordelis-Lo roof. It is certainly the most common problem to compare the various shell elements proposed in the literature. It is a circular cylindrical panel where the two curved edges are based on two rigid diaphragms alongside their plan and the other two edges are free. The panel is subjected to its own weight only. We give in Fig. 14 the geometrical and mechanical characteristics of the panel.

-	Length of the panel	L=6 m

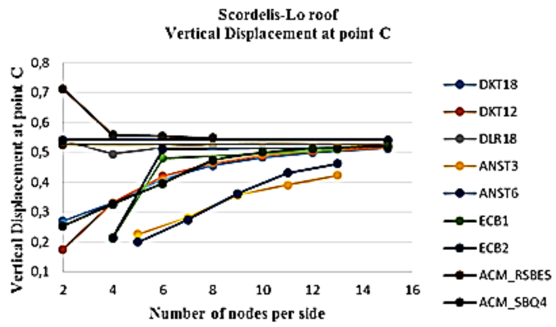

Fig. 15 Cylindrical panel subjected to its weight-vertical displacement at point C

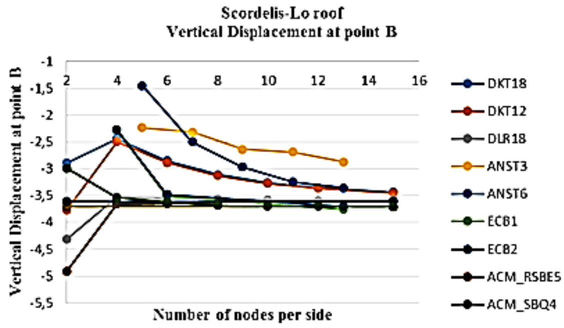

Fig. 16 Cylindrical panel subjected to its weight-vertical displacement at point B

-	Medium radius	R=3 m
-	Thickness of the panel	h=0.03 m
-	Young's Modulus	$E=30000\ N/m^2$
-	Poisson Coefficient	$\nu=0.03$
-	Volume weight of shell	$\gamma_g= -\ 0.2083\ N/m^3$
-	Angle	$\varphi= 40°$

Boundary conditions

$U=W=\Theta_Y=0$ Along AD

Symmetric conditions

$U= \Theta_Y = \Theta_z = 0$ Along CD

$V= \Theta_x = \Theta_z = 0$ Along CB

Reference values (Deep shell theory)

$W_B=-0.00361$ m $W_C= 0.000541$ m

Analytical solution (Shallow shell theory)

$W_B=-0.003703$ m $W_C= 0.000525$ m

$U_B=-0.001965$ m $V_A=-0.001513$ m

The panel is thin and shallow (R/h=100, L/h=200). The symmetry of the problem allows us to study only the ABCD quarter of the structure with regular meshes (N= 2, 4, 6 … elements) alongside AB and AD. We neglect the transverse shear deformations. The membrane deformations are more important than the bending deformation. The influence of the membrane on the overall behaviour of the shell is very dominant. Indeed, the comparison of the two effects (membrane and bending) at point (B) gives: $\frac{h\,N_x}{6\,M_x} = 4$. The results obtained by the present flat shell element for the vertical displacement at the mid-point B of the free edge, at the center C of the roof and for longitudinal displacement in A are shown in Figs. 15, 16 and 17 respectively. We compare our results with two reference solutions. The first

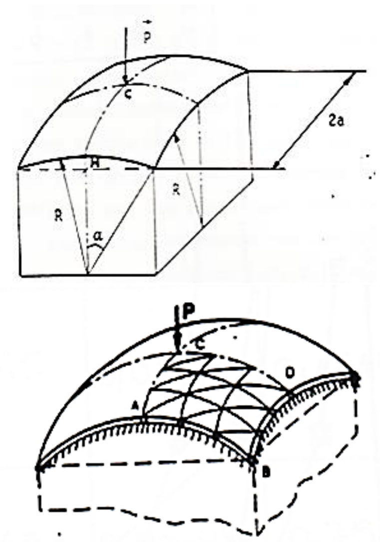

Fig. 17 Square base spherical shell-geometrical data and meshes

one is analytical and it is based on the shallow shell theory according to Scordelis (1964), and the second one is based on deep shell theory according to Forsberg (1970) on the one hand and numerical results cited in literature on the other hand. We see a rapid convergence of the present element to the shallow shell solution compared to other elements. This remarkable convergence is due to the richness of the element on the membrane (cubic interpolation). The convergence curves in Figs. 15, 16 and 17 show the good contribution of the strain-based approach. The overall results prove the good convergence of the present formulated shell element.

6.6 Square base spherical shell

The problem presented in Fig. 17 is the spherical shell, with a square base, articulated on its contour. The radius R, the opening α and the thickness define it. A concentrated load (P) is applied to the shell at its center. Fig. 17 presents the geometrical data and the mechanical characteristics of this shell. All edges of the shell are hinged.

Length of the square base (2a)	1569.8 mm
Radius of the sphere (R)	2540 mm
Young's Modulus (E)	68.95 MPa
Poisson Coefficient (υ)	0.3
Thickness (h)	99.45 mm
Load (concentrated P)	1.0 N

The results 2a/h=15.78 and R/h=25.54 indicate that the shell is moderately thin. The symmetry of the problem enables us to study only the quarter ABDC of the shell. This problem has been treated analytically by Leicester (1968) and numerically by several researchers such as Dhatt (1970), Gallagher (1975), Tahiani and Lachance (1975),

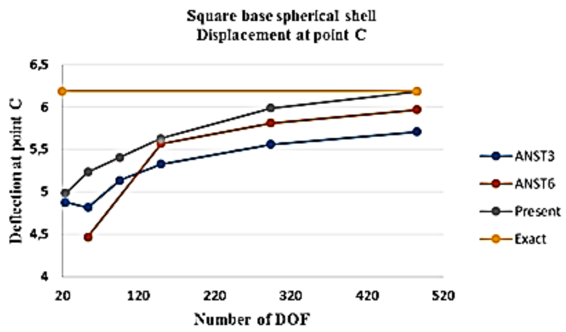

Fig. 18 Square base spherical shell-deflection at the center of the shell

Fezans (1981) and Guenfoud (1990). It is also quite low because the ratio of its depth to the length of its side is equal to 2a/H=12.65. The results obtained for the vertical displacements at the loading point (C) are shown in Fig. 18. The reference solution is taken from Fezans (1981). We observe a remarkable convergence of the present element for this example, which confirms the utility of our element even for structures with rather lower double curvature. Our element converges non-monotonously towards the solution of the lowered shells.

6.7 Hyperbolic paraboloid shell under uniform pressure

We consider a section of semi-thin hyperbolic paraboloid shell (2a/h=52) with clamped straight edges subjected to a uniform normal pressure. We show the geometrical data and mechanical properties of the material in Fig. 19. The equation governing the present shell example is given by: $\frac{Z}{C} = \frac{xy}{a^2}$.

Length (2a)	12.92
Elevation (C)	1.304
Young's Modulus (E)	5.10^5
Poisson Coefficient (υ)	0.39
Thickness (h)	0.25
Load (normal pressure q)	-1.0
All edges of shell are clamped	

The structure is not symmetrical so it is necessary to mesh the entire shell. The aim of the present example is to see the ability of our element to model double-curved structures. The present example is of slightly dominant bending. Indeed, at the point O and for z=h/2, we have: $\frac{6\,M_x}{h\,N_x} = 1.5$. We present the results of the study in Fig. 20. It characterizes the deflection at the centre as a function of the total number of degrees of freedom for different meshes. We compare our results with the analytical solution given by Chetty and Tottenham (1964) and then with the numerical solution given by Guenfoud (1990, 1996) and by Ben-Taher (1981). We note a good non-monotonic

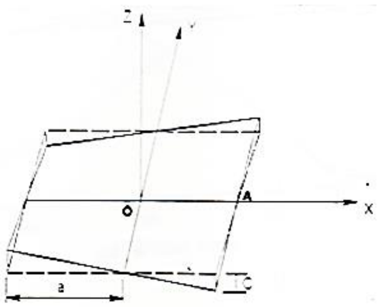

Fig. 19 Clamped hyperbolic paraboloid shell under-uniform pressure

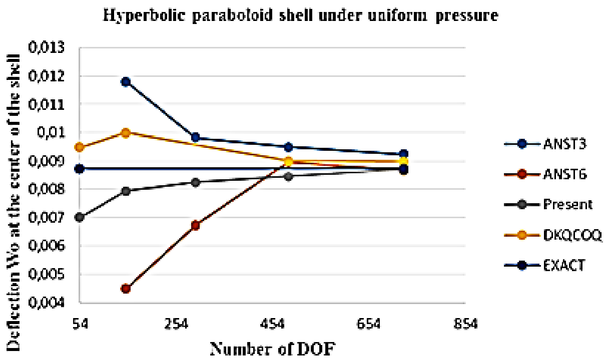

Fig. 20 Clamped hyperbolic paraboloid shell under-uniform pressure. Deflection at the center of the paraboloid

convergence of the results of our element towards the analytical solution.

6.8 Hemispherical shell problem (Mac neal test)

We study the hemispherical shell subjected to self-equilibrating radial point forces with 90° intervals, two inward and two outward forces at the quarter points of its open edges, via the quarter model shown in Fig. 21. This problem intends to pattern the element performance for the rigid body rotations and the nearby extensional bending of a doubly curved shell. We present the geometry and material properties in Fig. 21. Flugge (1960) offers the analytical solution for the problem. The reference solution for the radial displacement at the loaded points is 0.0924. Owing to symmetry, we analyze only a quarter of this hemispherical shell. We present the results for different mesh sizes in Fig. 22. They indicate that the proposed element performs well in comparison with other elements in the literature. We compare our results with the analytical solution given by Flugge (1960) and the reference solution by Belytchko (1984) and then with the numerical solution given by Guenfoud (1990, 1996).

Radius of the sphere (R)	10.00
Young's Modulus (E)	6.825×10^{7}
Poisson Coefficient (υ)	0.3
Thickness (h)	0.04
Load (concentrated F)	P=2

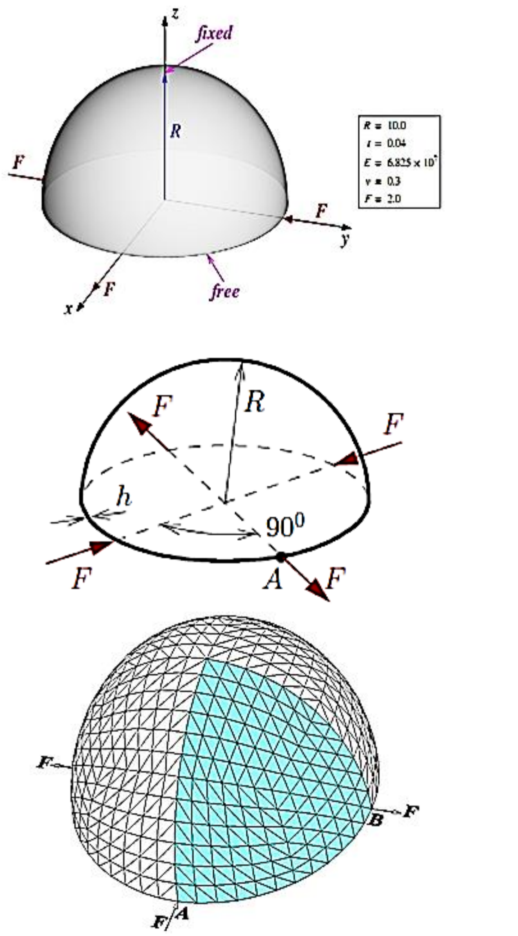

Fig. 21 Hemispherical shell problem (Mac Neal Test)-geometrical data and meshes

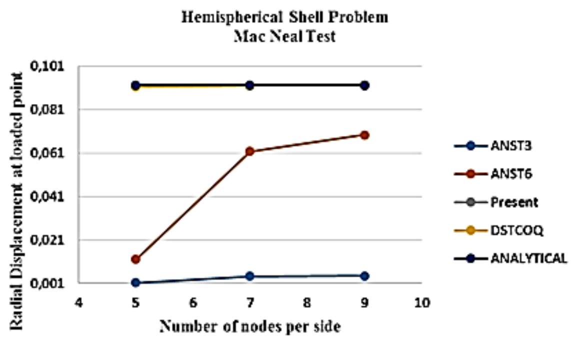

Fig. 22 Hemispherical shell problem (Mac Neal Test)-radial displacement at loaded point

5. Conclusions

The formulation of a flat triangular thin shell element with a true rotation based upon the strain approach has been successfully developed and presented in the present paper. The three translational displacements (u, v and w) are each described in terms of cubic polynomial functions. The use of equal-order fields for all displacements has the effect of approximating more strictly the rigid body motion condition. The originality in the formulation of the present element lies in the use of the model in deformation and the use of concepts and techniques in order to achieve:

- The enrichment of the fields of displacement (P refinement), thus a better precision in the approximation of the solution;
- Enhancement of behaviour in the case of geometric distortion of the meshes;
- The avoidance of the membrane-locking problem for curved structures;
- The response to the numerical problems induced by the absence of the rigidity related to the rotation around the normal in the case of the coplanar elements.

These concepts and techniques are:

- Adoption of the deformation approach;
- The introduction of a fourth internal node in the three-node triangular element;
- The reduction of elementary stiffness matrices using the static condensation technique;
- The use of analytical integration to evaluate the stiffness matrix.

This approach led us to a competitive, robust and efficient flat faceted shell element. The present formulation (strain approach) is demonstrated to be consistent in a very wide variety of linear analysis situations. A series of test problems were conducted to evaluate the efficiency of the element compared to other elements in the literature. The results obtained confirmed the fast convergence rate of the element. The proposed element has the advantage of being simple in form and uses the six degrees of freedom. Further, it can be used for the analysis of thin shell structures, even those with complex geometries.

Acknowledgments

The Higher Education Ministry financially supported the research described in this paper.

References

Abderrahmani, S., Maalam, T. and Hamadi, D. (2016), “On improved thin plate bending rectangular finite element based on the strain approach”, *Int. J. Eng. Res. Afr.*, **27**, 76-86.

Barik, M. and Mukhopadhyay, M. (2002), “A new stiffened plate element for the analysis of arbitrary plates”, *Thin-Wall. Struct.*, **40**(7), 625-639.

Batoz, J.L. (1977), “Analyse non linéaire de coques minces élastiques de formes arbitraires par éléments triangulaires courbes”, Thèse de Doctorat, Faculté des sciences et de génie civil, Québec, 372.

Batoz, J.L. and Dhatt, G. (1990), *Modélisation Des Structures Par Eléments Finis: Solides Elastiques*, Presses Université Laval, **1**.

Belarbi M.T. (2000), “Développement de nouveaux éléments à modèle en déformation: Application linéaire et non linéaire”, Thèse de Doctorat, Université de Constantine, Algérie.

Belarbi, M.T. and Charif, A. (1999), “Développement d'un nouvel élément hexaédrique simple basé sur le modèle en déformation pour l'étude des plaques minces et épaisses”, *Revue Européenne des éléments Finis*, **8**(2), 135-157.

Belytschko, T., Ong, J.S.J., Liu, W.K. and Kennedy, J.M. (1984), “Hourglass control in linear and nonlinear problems”, *Comput. Meth. Appl. Mech. Eng.*, **43**(3), 251-276.

Belytschko, T., Stolarski, H., Liu, W.K., Carpenter, N. and Ong, J.S. (1985), “Stress projection for membrane and shear locking in shell finite elements”, *Comput. Meth. Appl. Mech. Eng.*, **51**(1), 221-258.

Bentaher, M. (1981), “Analyse élastoplastique des plaques et coques minces par éléments finis”, Thèse de 3ème cycle, Université de Technologie de Compiègne, 130.

Bhothikhun, P. and Dechaumphai, P. (2014), “Adaptive DKT finite element for plate bending analysis of built-up structures”, *Int. J. Mech. Mechatron. Eng.*, **14**(1), 12-20.

Bonnes, G. (1969), “Analyse des Voiles Mz par éléments finis courbés”, Ph.D. Dissertation, Université Laval, Canada.

Boutagouga D. (2008), “Analyse non-linéaire géométrique et matérielle des coques par un élément quadrilatère avec ddl rotationnel dit (Drilling rotation)”, Mémoire de Magister, Université Badji mokhtar Annaba.

Boutagouga, D. and Djeghaba, K. (2016), “Nonlinear dynamic co-rotational formulation for membrane elements with in-plane drilling rotational degree of freedom”, *Eng. Comput.*, **33**(3), 667-697.

Boutagouga, D. (2016), “A new enhanced assumed strain quadrilateral membrane element with drilling degree of freedom and modified shape functions”, *Int. J. Numer. Meth. Eng.*

Boutagouga, D., Gouasmia, A. and Djeghaba, K. (2010), “Geometrically nonlinear analysis of thin shell by a quadrilateral finite element with in-plane rotational degrees of freedom”, *Eur. J. Comput. Mech./Rev. Eur. Mécan. Numér.*, **19**(8), 707-724.

Bouzriba, A. and Bouzrira, C. (2015), “Sector element for analysis of thick cylinders exposed to internal pressure and change of temperature”, *Građevin.*, **67**(6), 547-555.

Burkardt, J. (2010), *FEM Basis Functions for a Triangle*, <http://people.sc. fsu.edu/.../ cg_lab_fem_basis_triangle.pdf>.

Carpenter, N., Stolarski, H. and Belytschko, T. (1985), “A flat triangular shell element with improved membrane interpolation”, *Int. J. Numer. Meth. Biomed. Eng.*, **1**(4), 161-168.

Carpenter, N., Stolarski, H. and Belytschko, T. (1986), “Improvements in 3-node triangular shell elements”, *Int. J. Numer. Meth. Eng.*, **23**(9), 1643-1667.

Chetty, S. and Tottenham, H. (1964), “An investigation into the bending analysis of hyperbolic paraboloide shells”, *Ind. Concrete J.*, 248-258.

Chinosi, C. (2005), “PSRI elements for the Reissner-Mindlin free plate”, *Comput. Struct.*, **83**(31), 2559-2572.

Dhatt, G.S. (1970), “Instability of thin shells by the finite element method”, *Proc. IASS Symp.*, Vienna, Austria.

Donnell, L.H. (1933), *Stability of Thin Walled Tubes under Torsion*, NACA Report No. 479.

El-Khaldi, F. (1987), “Contribution au traitement des phenomenes de blocage de membrane et cisaillement dans la modelisation des arcs et des coques minces en theorie de marguerre”, Ph.D. Dissertation, Villeurbanne, INSA.

Fezans, G. (1981), “Analyse linéaire et non linéaire géométrique des coques par éléments finis isoparamétriques tridimensionnels dégénérés”, Ph.D. Dissertation.

Flűgge, W. (1960), *Stresses in Shells*, Springer Verlag, Berlin/Heidelberg/New York.

Forsberg, K. and Hartung, R. (1970), “An evaluation of finite difference and finite element techniques for analysis of general shells”, *Proceedings of the Symposium on High Speed Computation of Elastic Structures*, IUTAM, Liège, Belgium.

Forsberg, K. and Flügge, W. (1966), “Point load on a shallow elliptic paraboloid”, *J. Appl. Mech.*, **33**(3), 575-585.

Frey, F. (2000), *Analyse des Structures et Milieux Continus : Mécanique des Structures*, PPUR Presses Polytechniques.

Gallagher, R.H. (1975), “Shell elements”, *Proceedings of the 1st World Congress on Finite Element Methods in Structural*

Mechanics, Bournemouth, U.K.

Geoffroy, P. (1983), "Développement et évaluation d'un élément fini pour l'analyse non linéaire statique et dynamique de coques minces", Ph.D. Dissertation.

Gileva, L., Shaydurov, V. and Dobronets, B. (2013), "The triangular Hermite finite element complementing the Bogner-Fox-Schmit rectangle", *Appl. Math.*, **4**(12), 50.

Guenfoud, M. (2000), "A new three nodes shell element with transverse shear", *Eng. J. Qatar Univ.*, **13**, 193-221.

Guenfoud, M. (1990), "*Deux éléments Triangulaires Nouveaux pour L'analyse Linéaire et Non Linéaire Géomètrique des Coques*", Ph.D. Dissertation, Villeurbanne, INSA, France.

Guenfoud, M. (1993), "Présentation de l'élément DSTM pour le calcul linéaire des coques d'épaisseur quelconque", *Ann. ITBTP*, (515), 25-52.

Guenfoud, M. (1996), "A new three nodes shell element with transverse shear", *J. Int. Assoc. Shell Spat. Struct.*, **37**(3), 193-220.

Hamadi, D. (1989), "Numerical and experimental investigation of an elliptical parboloid thin shell structures", Ph.D. Dissertation, City University London, U.K.

Hamadi, D. (2006), "Analysis of structures by non-conforming finite elements" analyse des structures par elements finis non conformes", Ph.D. Dissertation, Université Mohamed Khider Biskra.

Hamadi, D., Ayoub, A. and Abdelhafid, O. (2016), "A new flat shell finite element for the linear analysis of thin shell structures", *Eur. J. Comput. Mech.*, 1-24.

Hamadi, D., Ayoub, A. and Maalem, T. (2016), "A new strain-based finite element for plane elasticity problems", *Eng. Comput.*, **33**(2), 562-579.

Himeur, M. (2008), "Développement d'éléments membranaires nouveaux d'élasticité plane basés sur la formulation en déformation", Ph.D. Dissertation, Thèse de magistère, Université de Guelma (Algérie), Département de Génie Civil.

Himeur, M. and Guenfoud, M. (2008), *Elément Fini Triangulaire Nouveau à Nœud Central Perturbé en Formulation Déformation Avec Drilling Rotation*, *CIFMA 3*, 21-23, Alep.

Himeur, M. and Guenfoud, M. (2011), "Bending triangular finite element with a fictitious fourth node based on the strain approach", *Eur. J. Comput. Mech./Rev. Eur. Mécan. Numér.*, **20**(7-8), 455-485.

Himeur, M., Benmarce, A. and Guenfoud, M. (2014), "A new finite element based on the strain approach with transverse shear effect", *Struct. Eng. Mech.*, **49**(6), 793-810.

Himeur, M., Zergua, A. and Guenfoud, M. (2015), "A finite element based on the strain approach using Airy's function", *Arab. J. Sci. Eng.*, **40**(3), 719-733.

Huang, M., Zhao, Z. and Shen, C. (2010), "An effective planar triangular element with drilling rotation", *Fin. Elem. Analy. Des.*, **46**(11), 1031-1036.

Jeon, H.M., Lee, P.S. and Bathe, K.J. (2014), "The MITC3 shell finite element enriched by interpolation covers", *Comput. Struct.*, **134**, 128-142.

Kim, D.N. and Bathe, K.J. (2009), "A triangular six-node shell element", *Comput. Struct.*, **87**(23), 1451-1460.

Ko, Y., Lee, Y., Lee, P.S. and Bathe, K.J. (2017), "Performance of the MITC3+ and the MITC4+ shell elements in widely-used benchmark problems", *Comput. Struct.*, **193**, 187-206.

Koiter, W. (1960), "A consistent first approximation in the general theory of thin elastic shells", *Theor. Thin Elast. Shells*, 12-33.

Koiter, W.T. and Simmonds, J.G. (1973), *Foundations of Shell Theory, Theoretical and Applied Mechanics*, Springer Berlin Heidelberg.

Kugler, S., Fotiu, P.A. and Murin, J. (2010), "A highly efficient membrane finite element with drilling degrees of freedom", *Acta Mech.*, **213**(3-4), 323-348.

Leicester, R.H. (1968), "Finite deformations of shallow shells (Shallow shell deformations based on nonlinear equations solved by Newton-Raphson iteration)", *Am. Soc. Civil Eng. Eng. Mech. Div. J.*, **94**, 1409-1423.

Lindberg, G.M., Olson, M.D. and Cowper, G.R. (1969), "New developments in the finite element analysis of shells", *Quarterly Bulletin of the Division of Mechanical Engineering and The National Aeronautical Establishment*, **4**, 1-38.

Papanicolopulos, S.A., Zervos, A. and Vardoulakis, I. (2009), "A three-dimensional C^1 finite element for gradient elasticity", *Int. J. Numer. Meth. Eng.*, **77**(10), 1396-1415.

Providas, E. and Kattis, M.A. (2000), "An assessment of two fundamental flat triangular shell elements with drilling rotations", *Comput. Struct.*, **77**(2), 129-139.

Rezaiee-Pajand, M. and Karkon, M. (2014), "Hybrid stress and analytical functions for analysis of thin plates bending", *Lat. Am. J. Sol. Struct.*, **11**(4), 556-579.

Rezaiee-Pajand, M. and Yaghoobi, M. (2014), "An efficient formulation for linear and geometric non-linear membrane elements", *Lat. Am. J. Sol. Struct.*, **11**(6), 1012-1035.

Sabir, A.B. (1985), "A rectangular and triangular plane elasticity element with drilling degrees of freedom", *Proceedings of the 2nd International Conference on Variational Methods in Engineering*.

Sanders, J.L. (1959), *An Improved First Approximation Theory for Thin Shells (NASA TR-R24)*, US Government Printing Office, Washington, U.S.A.

Sanders, Jr, J.L. (1959), *An Improved First-Approximation Theory for Thin Shells*.

Scordelis, A.C. and Lo, K.S. (1964), "Computer analysis of cylindrical shells", *J. Proc.*, **61**(5), 539-562.

Serpik, I.N. (2010), "Development of a new finite element for plate and shell analysis by application of generalized approach to patch test", *Fin. Elem. Analy. Des.*, **46**(11), 1017-1030.

Shin, C.M. and Lee, B.C. (2014), "Development of a strain-smoothed three-node triangular flat shell element with drilling degrees of freedom", *Fin. Elem. Analy. Des.*, **86**, 71-80.

Tahiani, C. and Lachance, L. (1975), "Linear and non-linear analysis of thin shallow shells by mixed finite elements", *Comput. Struct.*, **5**(2-3), 167-177.

Teodorescu, P. (1982), "Grands éléments finis GEF pour l'élasticité plane", Thèse no 462 de doctorat présentée au département de génie civil, Ecole polytechnique fédérale de Lausanne Suisse.

Thomas, G.R. and Gallagher, R.H. (1975), *A Triangular Thin Shell Finite Element: Linear Analysis*.

Timoshenko, S. and Woinowsky-Krieger, S. (1959), *Theory of Plates and Shells*, McGraw-Hill.

Zienkiewicz, O.C., Taylor, R.L., Zienkiewicz, O.C. and Taylor, R.L. (1977), *The Finite Element Method*, McGraw-Hill, London, U.K.

Zweiling, K. (1952), *Grundlagen Einer Theorie der Biharmonischen Polynome*, Verlag Technik.

PL